Manganese Oxides: Battery Materials Make the Leap to Electrochemical Capacitors

by Daniel Bélanger, Thierry Brousse, and Jeffrey W. Long

Manganese oxides have a relatively long history in the world of battery chemistry, dating back to the work of Leclanché in the 1860s, which ultimately formed the basis for the now-ubiquitous primary 1.5 V Zn/MnO_2 alkaline cell.[1] In the alkaline cell, manganese oxide (typically in the γ-MnO_2 form) serves as the active cathode material, and stores charge via the insertion of protons from the aqueous electrolyte, accompanied by reduction of Mn sites in the oxide by electrons from the external circuit, a complex process that can be represented by the simplified equation below (Eq. 1).

$$Mn^{IV}O_2 + x\ e^- + xH^+ \rightleftharpoons H_xMn^{III}{}_xMn^{IV}{}_{1-x}O_2 \quad (1)$$

With the ever-increasing power and energy needs of advanced consumer electronics and related technologies, more recent battery research and development has focused on rechargeable lithium and lithium-ion battery chemistries, which offer the advantages of higher voltages and higher energy densities. Manganese oxides (typically in the spinel $Li_{1-x}Mn_2O_4$ form) are also attractive cathode materials for lithium-ion batteries and have even been used in commercialized cells, for example in a 3.5 V $Li_xC/Li_{1-x}Mn_2O_4$ cell configuration.[2] As in the alkaline Zn/MnO_2 cell, charge storage occurs via cation/electron insertion, but in this case lithium cations are incorporated from a nonaqueous electrolyte (Eq. 2).

$$Mn^{IV}O_2 + x\ e^- + xLi^+ \rightleftharpoons Li_xMn^{III}{}_xMn^{IV}{}_{1-x}O_2 \quad (2)$$

The intense interest in manganese oxides for battery applications is driven by their low cost and low toxicity, particularly when compared to other metal oxides of relevance for batteries such as nickel- and cobalt-oxides. As a general class of materials, manganese oxides exhibit a very rich chemistry and can be synthesized in dozens of crystalline and disordered forms, each with distinctive physical and electrochemical properties. Thus from both a fundamental and practical perspective, manganese oxides provide a veritable "toolbox" of materials from which to select and optimize for particular electrochemical performance characteristics (stability, capacity, voltage, etc.). Although manganese oxides are complex, non-stoichiometric oxides, often containing additional metal cations, physisorbed and structural water, and structural vacancies, for the purposes of this article we will denote these materials generally as "MnO_2."

The use of manganese oxides for electrochemical energy storage has continued to expand to new applications, most recently to the field of electrochemical capacitors (ECs). Lee and Goodenough[3] initially reported that amorphous MnO_2 (a-MnO_2) powders, incorporated into composite electrode structures, exhibited a capacitor-like electrochemical response (*i.e.*, "pseudocapacitance") in mild aqueous electrolytes, and delivered a specific capacitance of 200 F g^{-1}. Since this initial report, interest in MnO_2 as an active material for ECs has grown steadily, as evidenced by the number of publications that have appeared on this subject in the refereed literature, beginning with six papers from 1999-2001, to more than 75 papers published from 2004-2007. The increasing worldwide interest in this area is based primarily on the anticipation that MnO_2 will ultimately serve as a low-cost alternative to disordered hydrous RuO_2,[4] which provides extremely high specific capacitance (>700 F g^{-1}), but at costs that are prohibitive for most applications.

In this article we assess the current status of manganese oxides with respect to their application in aqueous-electrolyte ECs, and discuss their future prospects from both a fundamental and applied perspective.

Materials and Electrode Structures

A survey of the recent literature reveals that the electrochemical performance of MnO_2 in EC configurations is determined by many variables, including the particle size of the MnO_2 and its crystal structure (or lack thereof), which are, in turn, determined by the synthetic methods (*e.g.*, sol–gel chemistry, electrodeposition, sputter deposition) and post-synthesis heat treatments used to produce the oxide. The morphology and microstructure of electrodes containing the MnO_2 phase, ranging from conventional composite electrodes to advanced nanostructured electrode architectures, is also critical, particularly in determining the high-rate performance of the resulting electrode structure. In the most common approach, high-surface-area MnO_2 powders are incorporated in conventional composite electrode structures containing carbon powder (for improved electronic conductivity) and a polymer binder, with the resulting electrodes delivering specific capacitances of ~125 to 250 F g^{-1}.[3,5] Micrometers-thick films of MnO_2 typically yield similar specific capacitance values,[6] although Nagarajan, *et al.*[7] and Shinomiya, *et al.*[8] have reported specific capacitances > 400 F g^{-1} for electrodeposited MnO_2 films.

Several groups have reported that when MnO_2 is formed as ultrathin (tens to hundreds of nanometers thick) films on planar current collectors, anomalously high gravimetric capacitances (~700 to 1380 F g^{-1}) can be observed.[9-11] Maintaining a nanoscopically thin MnO_2 film or coating in close proximity to the current collector overcomes the limitations of the poor electronic conductivity of MnO_2 (10^{-5}–10^{-6} S cm^{-1}) and also reduces the distances for the solid-state transport of insertion cations. The implications of these findings have been translated to 3-dimensional electrode designs in which nanoscopic MnO_2 deposits are incorporated directly onto the surface of nanostructured carbons, including carbon nanotubes,[12-15] templated mesoporous carbons,[16] and carbon aerogels/nanofoams (see Fig. 1).[17] In such a configuration, the nanostructured carbon substrate serves a high-surface-area, 3-D current collector for the MnO_2 coatings, and defines the internal pore structure of the electrode, which facilitates the infiltration and rapid transport of electrolyte to the nanoscopic MnO_2 phase. Although such 3D MnO_2-carbon nanostructures are still being optimized, preliminary results indicate that efficient utilization of the incorporated MnO_2 phase can be achieved. For example, Dong, *et al.*,[16] reported a specific capacitance of ~600 F g^{-1}, normalized to the MnO_2 content in a composite nanostructure with templated mesoporous carbon.

(continued from previous page)

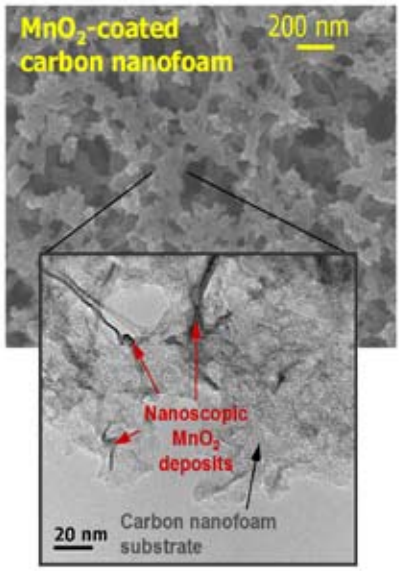

Fig. 1. *Scanning electron micrograph (top) and transmission electron micrograph (bottom) of a MnO_2-carbon nanofoam hybrid nanoarchitecture.*

Underlying Electrochemical Charge-Storage Mechanisms

A detailed knowledge of the charge-storage mechanism of MnO_2 is of the utmost importance in order to understand the factors that control the charge-storage process and to ultimately develop materials and electrode structures that demonstrate improved electrochemical performance. Some clues about the charge-storage mechanism can be found in the initial study of Lee and Goodenough,[3] where it was shown that the cyclic voltammetry behavior and the specific capacitance depends on the nature of the cations (Li^+, Na^+, K^+) in the electrolyte. The chemisorption of cations on the oxide surface, as well as the hydration sphere of the cation were thought to be important parameters. Therefore, a mechanism based on the surface adsorption of electrolyte cations (C^+) on MnO_2 can be described by:

$$(MnO_2)_{surface} + C^+ + e^- \Longleftrightarrow (MnO_2\text{-}C^+)_{surface} \quad (3)$$

where $C^+ = Na^+, K^+, Li^+$. Subsequently, Pang and Anderson[9] proposed that the reduction of MnO_2 to MnOOH involves the incorporation of protons and electrons into the oxide lattice:

$$MnO_2 + H^+ + e^- \Longleftrightarrow MnOOH \quad (4)$$

The relatively high charge-storage capacity of manganese dioxide is presumably due to facile proton diffusion into hydrous manganese dioxide films. In another study, they also proposed that alkali metal cations can intercalate/deintercalate within the oxide lattice during the redox process.[18]

$$MnO_2 + C^+ + e^- \Longleftrightarrow MnOOC \quad (5)$$

Although these early investigations suggested that redox cycling of the MnO_2 in mild aqueous electrolytes was responsible for the observed pseudocapacitance, this fact was not conclusively demonstrated until spectroscopic tools were applied to such systems.

Accordingly, X-ray photoelectron spectroscopy (XPS) has been used to determine whether a change of the manganese valence is observed upon charge/discharge of MnO_2 electrodes. In a recent study by Toupin, *et al.*, the Mn3s and O1s core level spectra were used to assess the change in oxidation state of manganese for a-MnO_2 electrodes that were oxidized and reduced at various potentials.[10] The energy separation between the two peaks of the Mn3s doublet (ΔEb) shows an inverse linear relationship with the manganese oxidation state, and thus can be used as an *ex-situ* probe of the MnO_2 redox process.[19] The ΔEb of the Mn3s components for the reduced a-MnO_2 thin film was found to be larger than that of the oxidized film and consistent with mean manganese oxidation state of 4 and 3 for the oxidized and reduced film electrodes, respectively (Fig. 2, left). Similarly, the observed variation of the O1s spectra is consistent with a similar change in the manganese oxidation state. However, in contrast to the thin film a-MnO_2 electrode, no change of the manganese oxidation state was observed for thick composite electrodes containing the same a-MnO_2 phase. The invariance of the manganese oxidation state for the composite electrode suggests that only a thin layer of MnO_2 is involved in the pseudocapacitance process (Fig. 2, right). In the same study, Na1s core level XPS spectra showed that the variation of the Na^+ content, expressed as the Na/Mn ratio, between the oxidized and the reduced electrodes does not track the charge transferred during the redox process. These results clearly demonstrate that protons are also involved in the redox process of MnO_2. Thus, these XPS data are consistent with a combination of mechanisms embodied in Eqs. 4 and 5.

Direct evidence for the variance of the manganese valence for a crystallized form of MnO_2 was recently shown by *in situ* X-ray absorption near-edge structure (XANES), where it was found that the main absorption edge, which is associated with the transition from Mn1s to p-like states, progressively shifted to lower energies upon electrochemical reduction of the MnO_2 electrode, in agreement with a decrease of the manganese valence.[20] In that study, a reversible expansion and shrinkage in lattice spacing of the oxide during charge transfer at manganese sites upon reduction/oxidation of MnO_2 was also demonstrated by *in-situ* synchrotron X-ray diffraction. This lattice expansion indicates that the pseudocapacitance of MnO_2 involves intercalation or insertion of cations into the bulk of the oxide structure and is not limited to only the surface in contact with the electrolyte. Similarly, an increase of the interlayer spacing of a crystallized birnessite-type manganese dioxide upon electrochemical oxidation in the presence of Na^+ cations in the electrolyte was recently reported and associated with the deintercalation of Na^+ and the intercalation of H_2O between the layers.[21]

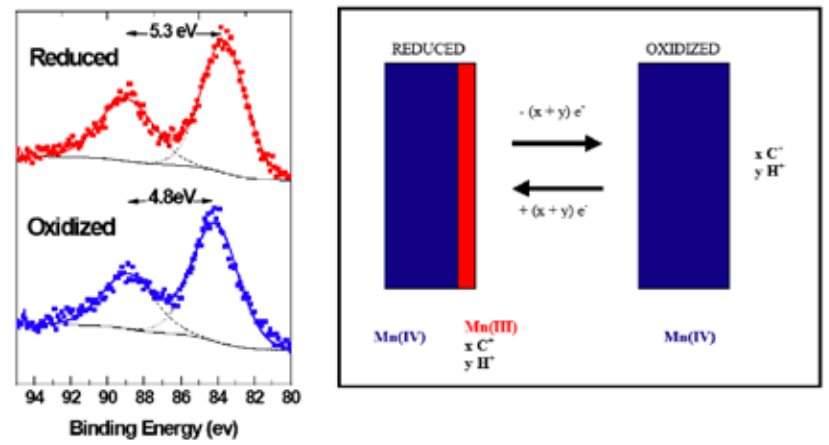

Fig. 2. *Mn3s core level spectra for reduced and oxidized MnO_2 electrodes (left) and schematic representations of the chemical processes and transformation involved in the charge/discharge (right).*

Table I. Summary of literature data on MnO_2-based asymmetric EC devices.

Negative electrode	Positive electrode	Current collector	Electrolyte salt	Cell voltage *V*	C* *F g^{-1}*	ESR* *Ω cm^2*	Energy Density* *W h kg^{-1}*	Power Density* *kW kg^{-1}*	Number of cycles	Ref.
AC	MnO_2	Titanium	KCl	2.0	52	—	28.8	0.5	100	22
MnO_2	MnO_2	SS	K_2SO_4	1.0	36	—	3.3	3.08	—	23
Fe_3O_4	MnO_2	SS	K_2SO_4	1.8	21.5	—	8.1	10.2	5,000	23
AC	MnO_2	SS	K_2SO_4	2.2	31	—	17.3	19	10,000	23
AC	MnO_2	Titanium	K_2SO_4	1.5	—	—	7.0	10	23,000	24
MnO_2	MnO_2	Gold	KNO_3	0.6	160	1.56	1.9	3.8	—	25
AC	MnO_2	Gold	KNO_3	2.0	140	0.54	21	123	1,000	25
PANI	MnO_2	Gold	KNO_3	1.2	—	0.57	5.86	42.1	500	26
Ppy	MnO_2	Gold	H_2SO_4	1.4	—	0.52	7.37	62.8	500	26
PEDOT	MnO_2	Gold	KNO_3	1.8	—	0.48	13.5	120.1	500	26
AC	MnO_2	Ni foam	LiOH	1.5	62.4	—	19.5	—	1,500	27
AC	$LiMn_2O_4$	Ni grid	Li_2SO_4	1.8	56	3.3	10.0	2	20,000	28
AC	MnO_2	SS	K_2SO_4	2.0	21	1.3	11.7	—	195,000	29

Abbreviations: activated carbon (AC), polyaniline (PANI), polypyrrole (Ppy), poly(3,4-ethylenedioxythiophene) (PEDOT), stainless steel (SS), capacitance (C), equivalent series resistance (ESR).
**See cited references for further details on experimental conditions and calculations.*

Toward Aqueous MnO_2-based Asymmetric Devices

The principal performance limitation of MnO_2-based ECs is the relatively narrow electrochemical window in which MnO_2 is stable. The upper cut-off voltage (≈ 0.9 V vs. Ag/AgCl) for MnO_2 is limited by the oxygen evolution reaction, which adds a non-reversible redox process to the pseudocapacitance process. Similarly, the lower cut-off voltage is determined by the onset of the Mn^{4+} "irreversible" reduction and subsequent manganese dissolution, which removes active material at each charge of the electrode. The specific lower potential value depends on the crystal structure and the microstructure of MnO_2. For standard "amorphous" powder, the lower cut-off voltage is close to -0.1 V vs. Ag/AgCl. Subsequently, the cell voltage of a symmetrical MnO_2/MnO_2 device hardly exceeds 1.0 V, which limits both energy and power densities and negates the beneficial effects of high specific capacitance values of this promising metal oxide.

One strategy to overcome the limited voltage window is to build asymmetric devices using a positive MnO_2 electrode and a different negative electrode, one with a useful electrochemical window complementary to MnO_2 (*i.e.*, with a lower cut-off potential below -0.1 V vs. Ag/AgCl). Only a few materials can satisfy this requirement, especially in mild aqueous electrolytes; among these are other metal oxides (*e.g.*, magnetite), conducting polymers (*e.g.*, poly-aniline, poly(3,4-ethylenedioxythiophene)), and carbon. Table I summarizes the performance of the different asymmetric EC devices, which can be divided into two categories.

The first category uses a faradaic or pseudocapacitive negative electrode together with a pseudocapacitive MnO_2 positive electrode. The second type of asymmetric device combines an activated carbon electrode to a pseudocapacitive MnO_2 electrode as negative and positive electrodes, respectively (Fig. 3). In this case, both the nature of the electrode materials and the nature of the charge-storage mechanisms are different on the negative and positive sides. From Table I, it can be seen that combining a positive MnO_2 electrode to these negative electrodes produces an increase of the cell voltage from about 1 V for symmetrical MnO_2(-)/MnO_2(+) EC up to more than 2.2 V for an activated carbon (-)/MnO_2(+) asymmetric device. Because of the expanded voltage range, the activated carbon(-)/MnO_2(+) combination[22] provides energy densities up to 28.8 Whkg^{-1} (normalized to the total active material mass), nearly one order of magnitude higher than that for symmetrical MnO_2 devices (1.9 to 3.3 Whkg^{-1}), and also significantly higher than conventional symmetric carbon/carbon ECs that utilize nonaqueous electrolytes.

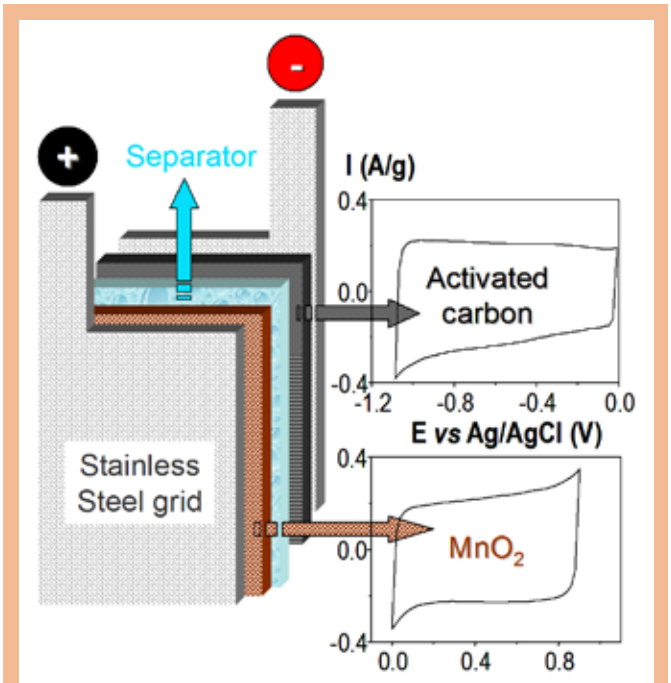

Fig. 3. *Schematic of an asymmetric EC using an activated carbon negative electrode (CV shown in insert) combined with a MnO_2 positive electrode (CV shown in insert) in 0.1 M K_2SO_4 electrolyte.*

The advantages of increased cell voltage and energy density for MnO_2-based aqueous asymmetric ECs must also be accompanied by long-term cycling stability of the resulting devices. The requirement for commercially viable ECs is between 100,000 and 1,000,000 cycles. Unfortunately, most of the MnO_2-based devices presented in the literature show only 100 to 1000 charge/discharge cycles, highlighting the difficulty to achieve long-term cycling stability for an asymmetric device, unlike the symmetrical carbon/carbon EC, which can sustain several hundred thousand cycles.

Two factors strongly influence the cycle life of the manganese dioxide electrode: (i) manganese dissolution, which leads to a progressive loss of active material and a subsequent capacitance fade upon cycling, and (ii) the oxygen evolution reaction, which can affect the electrode/current collector interface and exacerbate corrosion problems, ultimately increasing the equivalent series resistance (ESR) of the cell. For practical cells, it is important to carefully balance the weight and capacitance of the positive and negative electrodes in order to ensure that MnO_2 does not exceed its stable electrochemical window. For example, the potential of an a-MnO_2 electrode must be maintained between 0 and 0.9 V vs. Ag/AgCl upon cycling. The problem is even more challenging when a pseudocapacitive or faradaic negative electrode is used in combination with MnO_2, in which case, both electrodes have to be carefully monitored in order to avoid capacitance fade upon cycling. Practically, these devices have to be operated within a "safe" cell voltage range, which often results in a limited energy density. In the case of an activated carbon(-)/MnO_2(+) asymmetric EC, the stability of the carbon electrode is a less critical issue. Indeed, up to 195,000 cycles have been reported for such a device in which precautions were taken to limit the corrosion of the electrode/stainless steel current collector interface.[29]

Future Challenges and Opportunities for MnO_2-based ECs

The incorporation of MnO_2 electrodes into asymmetric cell configurations opens the way for safe aqueous-based ECs that deliver technologically relevant power and energy densities. Aqueous-based ECs present several advantages for device manufacturing: low-cost and environmentally friendly materials and components, no need for special atmospheres during cell assembly, and the use of simple nontoxic salts (*e.g.* Na_2SO_4). A 620 F activated carbon (-)/MnO_2(+) asymmetric device was recently assembled using this technology.[29] Additionally, the thermal management of aqueous-based asymmetric ECs was compared to standard carbon/carbon acetonitrile-based devices, and the superiority of the aqueous device was demonstrated due to higher thermal safety because of a higher vaporization temperature and non-flammability of the cell components, especially the aqueous electrolyte.

The design of optimized MnO_2-carbon nanoarchitectures for the positive electrode, as well as a more detailed understanding of charge-storage mechanisms in such composite materials will increase the performance of next-generation asymmetric EC devices. Apart from the scientific quest for high capacitance MnO_2-based active materials and the search of pertinent complementary negative electrode, the long-term cycling stability of MnO_2 is a technological issue that must be addressed in the near future in order to evaluate and validate the commercial development of aqueous-based asymmetric ECs. Other issues such as self-discharge, corrosion of the current collector, and low-temperature performances should also be examined. Considering that MnO_2-based EC technology is still in its infancy, future research and development should ultimately yield high-performance, low-cost, and safe energy-storage devices for applications with challenging energy/power requirements.

References

1. Y. Chabre and J. Pannetier, *Prog. Solid State Chem.*, **23**, 1 (1995).
2. M. Thackeray, *Prog. Solid State Chem.*, **25**, 1 (1997).
3. H. Y. Lee and J. B. Goodenough, *J. Solid State Chem.*, **144**, 220 (1999).
4. J. P. Zheng, P. J. Cygan, and T. R. Jow, *J. Electrochem. Soc.*, **142**, 2699 (1995).
5. H. Y. Lee, S. W. Kim, and H. Y. Lee, *Electrochem. Solid-State Lett.*, **4**, A19 (2001).
6. J.-K. Chang and W. T. Tsai, *J. Electrochem. Soc.*, **150**, A1333 (2003).
7. N. Nagaran, H. Humadi, and I. Zhitomirsky, *Electrochim. Acta*, **51**, 3039 (2006).
8. T. Shinomiya, V. Gupta, and N. Miura, *Electrochim. Acta*, **51**, 4412 (2006).
9. S.-C. Pang, M. A. Anderson, and T. W. Chapman, *J. Electrochem. Soc.*, 147, **444** (2000).
10. M. Toupin, T. Brousse, and D. Bélanger, *Chem. Mater.*, **16**, 3184 (2004).
11. J. N. Broughton and M. J. Brett, *Electrochim. Acta*, **49**, 4439 (2004).
12. V. Subramanian, H. Zhu, and B. Wei, *Electrochem. Commun.*, **8**, 827 (2004).
13. E. Raymundo-Piñero, V. Khomenko, E. Frackowiak, and F. Béguin, *J. Electrochem. Soc.*, **152**, A229 (2005).
14. C. Y. Lee, H. M. Tsai, H. J. Chuang, S. Y. Li, P. Lin, and Y. T. Tseng, *J. Electrochem. Soc.*, **152**, A716 (2005).
15. Y.-T. Wu and C.-C. Hu, *J. Electrochem. Soc.*, **151**, A2060 (2004).
16. X. Dong, W. Shen, J. Gu, L. Xiong, Y. Zhu, H. Li, and J. Shi, *J. Phys. Chem. B*, **110**, 6015 (2006).
17. A. E. Fischer, K. A. Pettigrew, D. R. Rolison, R. M. Stroud, and J. W. Long, *Nano Lett.*, **7**, 281 (2007).
18. S.-F. Chin, S.-C. Pang, and M. A. Anderson, *J. Electrochem. Soc.*, **149**, A379 (2002).
19. M. Chigane and M. Ishikawa, *J. Electrochem. Soc.*, **147**, 2246 (2000).
20. S.-L. Kuo and N.-L. Wu, *J. Electrochem. Soc.*, **153**, A1317 (2006).
21. L. Athouël, F. Moser, R. Dugas, O. Crosnier, D. Bélanger, and T. Brousse, *J. Phys. Chem. C*, accepted for publication.
22. M. S. Hong, S. H. Lee, and S. W. Kim, *Electrochem. Solid-State Lett.*, **5**, A227 (2002).
23. T. Cottineau, M. Toupin, T. Delahaye, T. Brousse, and D. Bélanger, *Appl. Phys. A - Mater.*, **82**, 599 (2006).
24. T. Brousse, M. Toupin, and D. Bélanger, *J. Electrochem. Soc.*, **151**, A614 (2004).
25. V. Khomenko, E. Raymundo-Piñero, and F. Béguin, *J. Power Sources*, **153**, 183 (2006).
26. V. Khomenko, E. Raymundo-Piñero, E. Frackowiak, and F. Béguin, *Appl. Phys. A - Mater.*, **82**, 567 (2006).
27. A. Yuan and Q. Zhang, *Electrochem. Comm.*, **8**, 1173 (2006).
28. Y. Wang and Y. Xia, *J. Electrochem. Soc.*, **153**, A450 (2006).
29. T. Brousse, P.-L. Taberna, O. Crosnier, R. Dugas, P. Guillemet, Y. Scudeller, Y. Zhou, F. Favier, D. Bélanger, and P. Simon, *J. Power Sources*, **173**, 633 (2007).

About the Authors

Daniel Bélanger is a professor at "l'Université du Québec à Montréal." He received his PhD from INRS-Énergie et Matériaux in 1985. His research interest includes the synthesis and characterization of new materials for energy conversion, sensors, and environmental chemistry. He may be reached at belanger.daniel@uqam.ca.

Thierry Brousse is a professor at Polytech Nantes (France) and Director of the Laboratoire de Génie des Matériaux et Procédés Associés (Materials Engineering, Energy, Metallurgy, Embrittlement, Welding, and Thermal Science) at the University of Nantes. His main research area is materials and devices for energy storage. He received his engineering degree from ISMRa in 1987 and his PhD in materials science from the University of Caen in 1991. He may be reached at thierry.brousse@univ-nantes.fr.

Jeffrey Long is a staff scientist in the Surface Chemistry Branch at the U.S. Naval Research Laboratory in Washington, DC, where his research is centered on the design, synthesis, and evaluation of nanostructured materials for electrochemical power sources, separation/filtration, and sensing. Before coming to the NRL, he received a PhD in chemistry from the University of North Carolina in 1997 and a BS from Wake Forest University in 1992. He may be reached at jeffrey.long@nrl.navy.mil.